Applied Energy 180 (2016) 834–848

Contents lists available at ScienceDirect

Applied Energy

journal homepage: www.elsevier.com/locate/apenergy

A numerical analysis of a composition-adjustable Kalina cycle power plant for power generation from low-temperature geothermal sources

Enhua Wang, Zhibin Yu *

School of Engineering, University of Glasgow, Glasgow G12 8QQ, UK

HIGHLIGHTS

- A composition-adjustable Kalina cycle is analysed and presented.
- An air-cooled condenser is used and thermodynamic performance is analysed.
- Composition adjustment can improve system performance significantly.

ARTICLE INFO

Article history:
Received 2 June 2016
Received in revised form 1 August 2016
Accepted 4 August 2016
Available online 13 August 2016

Keyword:
Kalina cycle
Dynamic power cycle
Composition adjustable
Ammonia-water mixture
Air-cooled condenser

ABSTRACT

The Kalina cycle is believed to be one of the most promising technologies for power generation from low temperature heat sources such as geothermal energy. So far, most Kalina cycle power plants are designed with a working fluid mixture having a fixed composition, and thus normally operate at a fixed condensing temperature. However, the ambient temperature (i.e., heat sink) varies over a large range as the season changes over a year, particularly in continental climates. Recently, a new concept, i.e., composition-adjustable Kalina cycle, was proposed to develop power plants that can match their condensing temperature with the changing ambient conditions, aiming at improving the cycle's overall thermal efficiency. However, no detailed analysis of its implementation and the potential benefits under various climate conditions has been reported. For this reason, this paper carried out a comprehensive numerical research on its implementation and performance analysis under several different climate conditions. A mathematical model is firstly established to simulate the working principle of a composition-adjustable Kalina cycle, based on which a numerical program is then developed to analyse the cycle's performance under various climate conditions. The developed numerical model is verified with some published data. The dynamic composition adjustment in response to the changing ambient temperature is simulated to evaluate its effect on the plant's performance over a year. The results show that a composition-adjustable Kalina cycle could achieve higher annual-average thermal efficiency than a conventional one with a fixed mixture composition. However, such an improvement of thermal efficiency strongly depends on the heat source temperature, climate conditions, etc. The composition-adjusting system introduces extra capital and operation costs. The economic viability of a composition-adjustable Kalina cycle power plant depends on the balance between these extra costs and the increase of thermal efficiency.

1. Introduction

Reducing fossil fuel consumption and greenhouse gas emissions is particularly important for us to ensure a sustainable future. Power generation from a variety of renewable heat sources such as geothermal and solar thermal energy could make an important contribution to the decarbonisation of our economy [1,2]. In particular, low-temperature geothermal energy is being used increasingly for power and heat generation [3]. Power cycles utilising low temperature heat sources have been intensively studied and well documented in the past several decades [4–6], amongst which organic Rankine cycles and Kalina cycles are considered to be two most important technologies [7,8].

In 1984, Kalina proposed a power cycle using a binary mixture as working fluid to generate power from heat source with a relatively low temperature, denoted as Kalina cycle later on [9]. The Kalina cycle is essentially a further development of Rankine cycle. One key difference between them is that a Kalina cycle uses a mixture rather than a pure working fluid, so that isobaric

* Corresponding author.
E-mail address: Zhibin.Yu@glasgow.ac.uk (Z. Yu).

http://dx.doi.org/10.1016/j.apenergy.2016.08.032
0306-2619/

Nomenclature

$\dot{E}$	exergy (kW)
h	enthalpy (kJ/kg)
$\dot{I}$	exergy destruction rate (kW)
$\dot{m}$	mass flow rate (kg/s)
P	pressure (MPa)
$\dot{Q}$	heat quantity (kW)
s	entropy (kJ/kg K)
T	temperature (K)
$\dot{W}$	power (kW)
x	ammonia mass fraction

Greek letters

η	efficiency
ψ	improvement of Cycle A relative to Cycle B

Subscripts

0	ambient condition
A, *B*	Cycles A, B
c	condenser
d	exergy destruction
e	evaporator
ex	exergy
f	fan
in	inlet
*m*1	Mixer 1
*m*2	Mixer 2
mix	mixture of the basic solution
n	net
out	outlet
*p*1	Pump 1
*p*2	Pump 2
re	recuperator
s	isentropic
*s*1	Separator 1
*s*2	Separator 2
t	turbine
th	thermal efficiency
tot	total
v	expansion valve

Acronyms

KCS	Kalina cycle system
KSG	Siemens' Kalina cycle system
OOL	optimal operation line
ORC	organic Rankine cycle
PPTD	pinch point temperature difference

evaporation and condensation processes occur under changing temperatures and the mixture composition varies throughout the cycle. Compared with a Rankine cycle, the efficiency of a Kalina cycle can be increased due to a close temperature match with heat transfer fluids in the evaporator and condenser. For instance, a Kalina cycle system using an ammonia-water mixture as the working fluid to generate power from the waste heat of a gas turbine achieved a thermal efficiency of 32.8% [10]. A Kalina power plant normally uses components (turbine, pumps, valves, etc.) similar to those for constructing a conventional steam power plant. Some investigations showed that a Kalina cycle can achieve a better thermal efficiency than ORC systems [11–14].

The Kalina cycle attracted considerable attention in the past decades. Fallah used an advanced exergy method to analyse a Kalina cycle (denoted as KCS-11 hereafter) for utilising a low-temperature geothermal source [15]. Cao et al. investigated a biomass-fuelled Kalina cycle system with a regenerative heat exchanger, and found the net power output and system efficiency increases as the temperature within the separator increases [16]. The performance of a KCS-11 system for solar energy application has also been studied. It was reported that the ammonia mass fraction was an important system operation parameter and should be optimised to reduce the system's irreversibility [17]. Recently, Yu et al. studied a combined system consisting of a Kalina power cycle and an ammonia absorption cooling cycle, of which the cooling to power ratio can be adjusted over a large range. Their theoretical results showed that the overall thermal efficiency could be increased by 6.6% by combining the two cycles in this way [18]. Wang et al. studied a flash-binary geothermal power generation system using a Kalina cycle to recover the heat rejection of a flash cycle [19]. The optimised results showed that the ammonia mass fraction, the pressure, and the temperature at the inlet of the turbine have significant effect on system's performance. Hettiarachchi et al. studied the performance of the KCS-11 Kalina cycle system for utilising low-temperature geothermal heat sources and found an optimum ammonia concentration exists for a given turbine inlet pressure [20].

Aiming at low-temperature heat sources, Kalina et al. proposed a power cycle which was later named KCS-34 [21], based on which a low-temperature geothermal power plant was built in Husavik, Iceland in 2000 [22]. Nasruddin et al. simulated a KCS-34 Kalina cycle using Cycle Tempo 5.0 software and compared it with the operation data of the Husavik power plant, showing a good agreement [23]. Later, Arslan studied the performance of a KCS-34 Kalina cycle system using an artificial neural network and life cycle cost analysis, and found that the most profitable condition was obtained when the ammonia mass fraction was in the range between 80% and 90% [24].

In practice, the expansion ratio of the turbine for KCS-34 cycle is relatively high and a multi-stage turbine is required. However, Lengert changed the location of the recuperator in a KCS-34 Kalina cycle and proposed a new power cycle, i.e., the so-called KSG-1 patented by Siemens. It can achieve high cycle efficiency and only requires a single-stage turbine [25]. Later on, Mergner and Weimer compared the thermodynamic performances between a KSG-1 and KCS-34 for geothermal power generation. The results showed that the KSG-1 achieved a slightly higher efficiency than the KCS-34 [26]. The architectures of KCS-11, KCS-34, and KSG-1 are compared and shown in Fig. 1.

In the past decade, different approaches have been proposed to further improve the efficiency of Kalina cycle power plants. Ibrahim and Kovach studied a method for controlling the temperature in the separator to adjust the ammonia mass fraction at the inlet of the turbine, and found that this method can improve the cycle's thermal efficiency [27]. Nguyen et al. developed a Kalina split-cycle that had a varying ammonia concentration during the pre-heating and evaporation processes [28]. He et al. studied two modified KCS-11 systems, which used a two-phase expander to replace a throttle valve [29]. Hua et al. investigated the transient performance of a Kalina cycle for high-temperature waste heat recovery, which can regulate the concentration of the working fluid mixture. This method controls the on/off state of two valves to maximise power generation when the temperature of the waste heat source fluctuates. Controlling the concentration of the working solution adjusts the turbine inlet pressure. It was reported that the cycle's

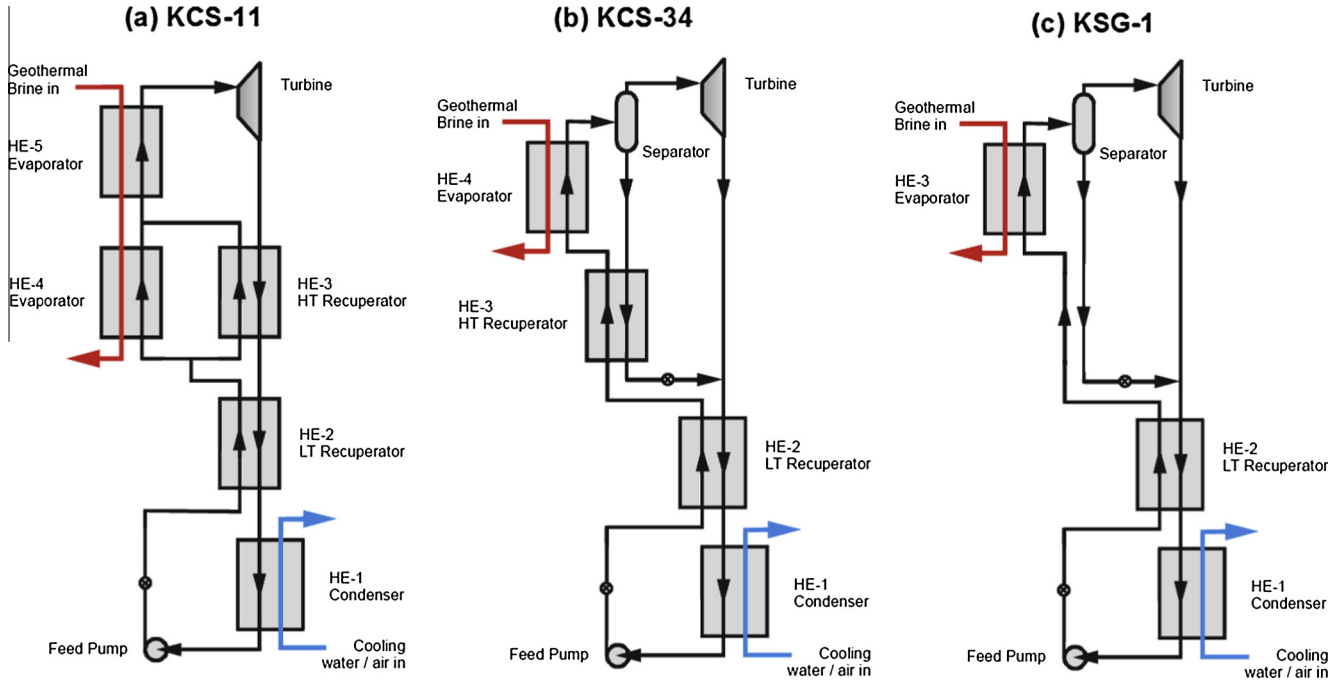

Fig. 1. Schematic of different Kalina cycle systems.

thermal efficiency was 12.8% greater than that of a conventional method [30].

Recently, Mlcak and Mirolli proposed a method to adjust the ammonia concentration according to the cooling source temperature to improve cycle efficiency [31]. A low-pressure separator is used at the upstream of the condenser to separate the two-phase mixture into an ammonia-rich vapour flow and an ammonia-lean liquid flow. Then, a drain pump is used to control the mass flow of the lean liquid mixture so that the ammonia mass fraction of the basic solution entering the condenser can be regulated. A density sensor is installed at the maximum pressure position of the basic solution to monitor the ammonia mass fraction in real time, which is sent to the controller as a feedback signal.

The thermodynamic principle of the proposed composition-adjustable Kalina cycle is considered to be technically feasible, but no details have been provided with regard to the implementation of such a power cycle and the potential improvement of the cycle's thermal efficiency under real climate conditions. Moreover, no further research has been reported on this subject according to our literature review. Apparently, there is a need for more insights of the proposed composition-adjustable Kalina cycle to further assess its technical and economic viabilities.

For this reason, this paper carried out a comprehensive numerical analysis of a composition-adjustable KSG-1 Kalina cycle power plant. The main objective is to answer several important questions as follows: (1) How can it be implemented? (2) How much can it improve the annual average thermal efficiency under various climate conditions? (3) What are the key factors affecting its performance?

Moreover, although most Kalina cycle power plants in operation usually use water-cooled condensers, large quantity of water may be not available or too costly, especially for an inland area [32,33]. It is then necessary to use air-cooled condensers, which are more sensitive to changing ambient temperatures. In order to maximise the effect of the ambient temperature change on the cycle's performance, an air-cooled condenser is employed for the system investigated in this research.

A theoretical model is firstly established, based on which a numerical code is developed. The effect of ammonia concentration on the system's performance is analysed. A case study based on Beijing's climate data has been carried out to demonstrate the performance improvement of the composition-adjustable Kalina cycle system. Finally, a brief performance comparison is performed for various types of climate conditions. The results show that the composition-adjustable Kalina cycle system can remain in the high-efficiency regions when the ambient temperature varies. Therefore, the system's performance can be improved.

2. Composition-adjustable Kalina system

Based on the concept proposed in a recent patent [31], a composition-adjustable KSG-1 Kalina cycle for low-temperature geothermal power generation is modelled in this study, of which the system architecture is shown in Fig. 2. An ammonia-water mixture is used as the working fluid. As ammonia and water have very different boiling temperatures, the gliding temperature of ammonia-water mixture is large and it can be used to decrease the irreversible losses during heat transfer processes in the condenser and evaporator. Fig. 3 shows the bubble and dew lines of ammonia-water mixture at a pressure of 2 MPa. When the ammonia mass fraction is 0.8, the bubble and dew temperatures are around 60.3 and 147.3 °C, respectively; the corresponding glide temperature is as large as 86.9 °C.

As shown in Fig. 2, the basic solution at the saturated liquid (state 1) enters Tank 1. A density sensor is installed at its outlet to measure the density of the ammonia-water mixture so that its composition can be deduced and used as a feedback signal for composition control. The low-pressure basic solution at state 3 is pressurised by Pump 1 and it turns into subcooled liquid at state 4. The basic solution is heated to state 5 by the recuperator. In the evaporator, the basic solution is further heated to a two-phase state 6 by a geothermal brine. For the convenience of comparison with the data in literature [25], the temperature of the brine water is set as 120 °C in this research. As the temperature is not high enough for the brine water to fully evaporate the basic solution,

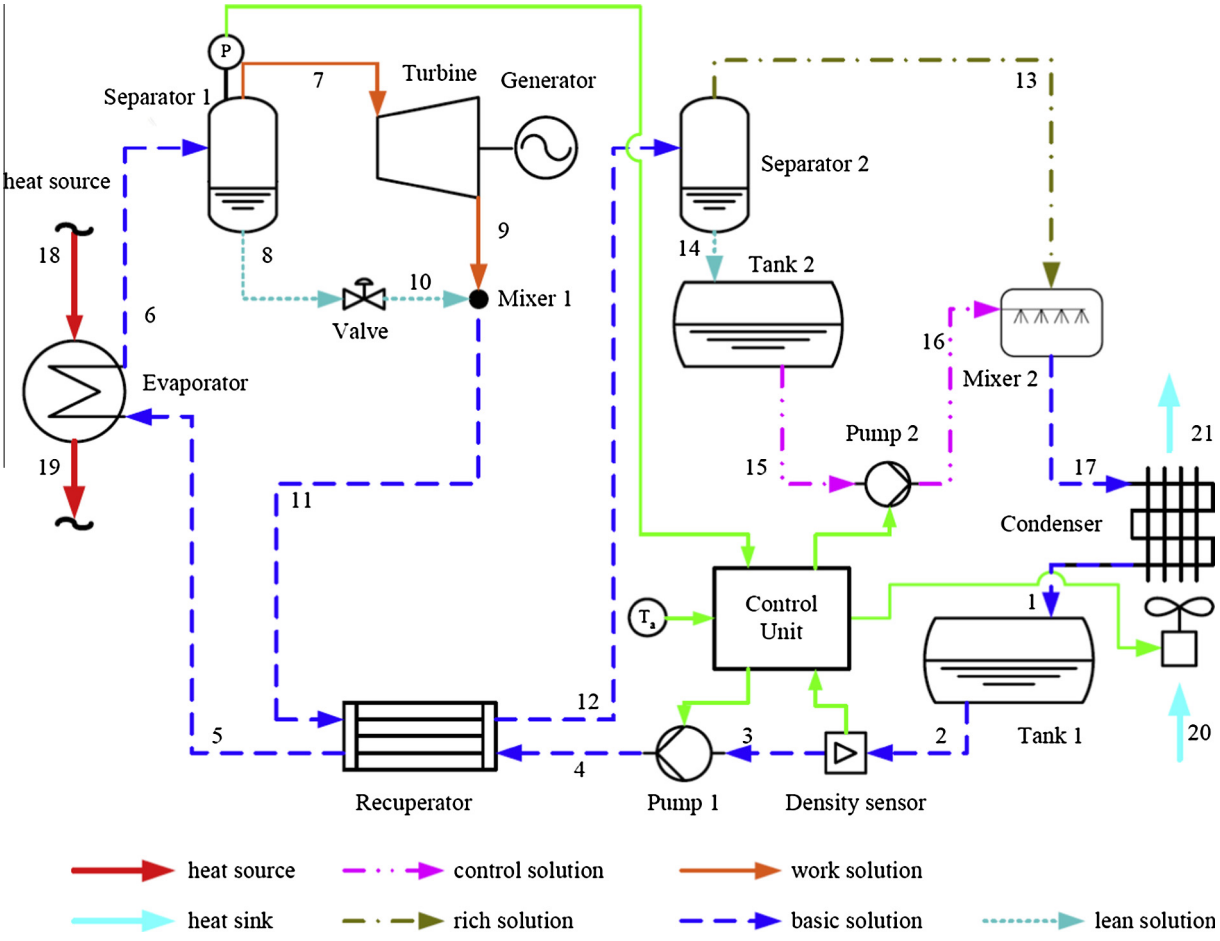

Fig. 2. Schematic of a composition-adjustable Kalina cycle for low-temperature geothermal power generation.

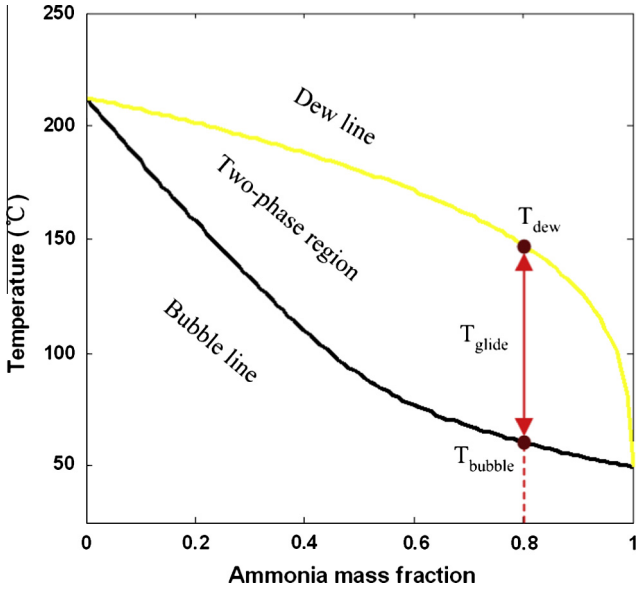

Fig. 3. Dew and bubble lines of ammonia-water mixture at a pressure of 2 MPa.

Separator 1 has to be used to separate the two-phase solution into an ammonia-rich saturated vapour mixture of state 7 (also called as the work solution) and an ammonia-lean saturated liquid mixture of state 8. The high-enthalpy vapour mixture expands in the turbine and turns into a low-pressure mixture at state 9. Meanwhile, the high-pressure liquid at state 8 is throttled through the expansion valve to state 10 to reduce its pressure. Subsequently, these two low-pressure flows are mixed to a two-phase state 11 in Mixer 1. It then flows into the recuperator, where the temperature of the low-pressure ammonia-water mixture decreases further after transferring its heat to the high-pressure side.

In order to improve the condensation process of ammonia-water mixture in the condenser, Separator 2 is employed to separate the two-phase flow (state 12) into saturated vapour (state 13) and saturated liquid (state 14). The liquid stream from Tank 2 is then pressurised by Pump 2 and sprayed into Mixer 2, further condensing the ammonia-rich vapour stream. The mixture is cooled and condensed in the condenser, turning into the saturated liquid (state 1).

The corresponding T-s and h-x diagrams are given in Fig. 4, where the numbers are the corresponding states as shown in Fig. 2. The black dashed lines represent the bubble lines of states 8 and 14, respectively; while the yellow dashed lines are the dew lines of states 7 and 13, respectively. It can be seen that the temperature glides during the processes 5-6, 11-12, and 17-1.

For the composition-adjustable Kalina cycle system as shown in Fig. 2, the control unit detects the pressure of the work solution in Separator 1 as a feedback signal to regulate the mass flow rate of Pump 1. The temperature of the basic solution at the inlet of Pump 1 is detected to control the air mass flow rate. The density of the basic solution at the inlet of Pump 1 is adjusted by varying the mass flow rate of Pump 2.

In this composition-adjustable Kalina cycle system, the density sensor is installed at the inlet of Pump 1 rather than at the outlet of

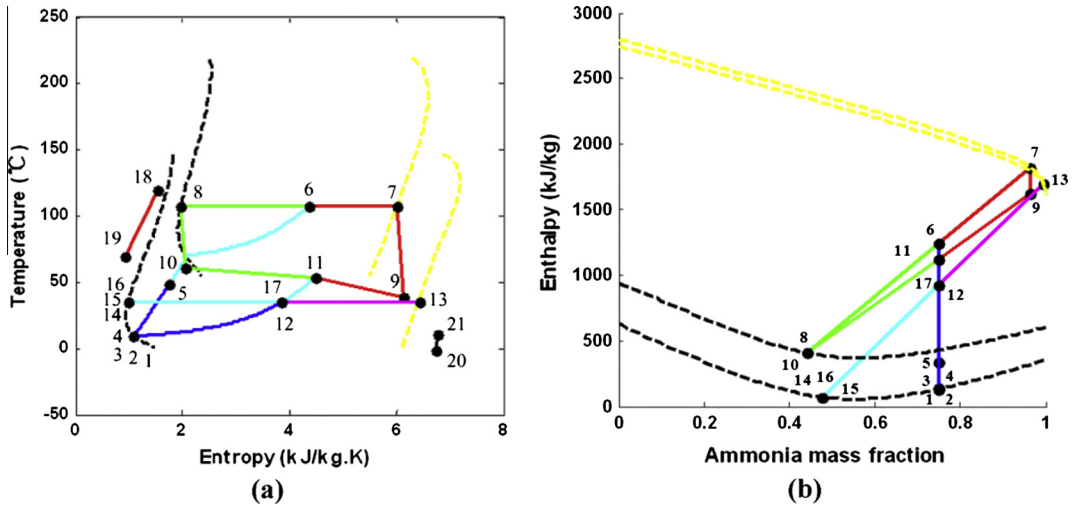

Fig. 4. Phase diagrams of the composition-adjustable Kalina cycle: (a) T-s diagram, (b) h-x diagram.

Pump 1 as proposed in Mlcak and Mirolli's patent [31]. Hereby, the operating pressure of the density sensor can be reduced. Furthermore, in Mlcak and Mirolli's patent, the system thermal efficiency is used as the performance indicator to optimise the ammonia mass fraction. However, in this paper, both the thermal efficiency and the exergy efficiency are used as the performance indicators.

3. Numerical modelling and validation

To evaluate the thermodynamic performance of the composition-adjustable Kalina cycle system, a mathematical model is established based on the mass and energy balance equations.

The power consumed by Pump 1 can be expressed as

$$\dot{W}_{p1} = \dot{m}_3(h_4 - h_3) = \dot{m}_3(h_{4s} - h_3)/\eta_p. \quad (1)$$

where process $3 \rightarrow 4$ s is the corresponding isentropic pumping process of process $3 \rightarrow 4$.

The heat transfer in the recuperator is determined by

$$\dot{Q}_{re} = \dot{m}_4(h_5 - h_4) = \dot{m}_{11}(h_{11} - h_{12}). \quad (2)$$

The heat transfer in the evaporator is modelled as

$$\dot{Q}_e = \dot{m}_5(h_6 - h_5) = \dot{m}_{water}(h_{18} - h_{19}). \quad (3)$$

For Separator 1, the equations of the ammonia mass fraction, the total mass, and the energy are represented by

$$\dot{m}_6 x_6 = \dot{m}_7 x_7 + \dot{m}_8 x_8, \quad (4)$$
$$\dot{m}_6 = \dot{m}_7 + \dot{m}_8, \quad (5)$$
$$\dot{m}_6 h_6 = \dot{m}_7 h_7 + \dot{m}_8 h_8. \quad (6)$$

Here, x_i is the ammonia mass fraction at state i. The ratio of the mass flow rate of state 7 to the total mass flow rate at state 6 is defined as

$$r_H = \frac{x_6 - x_8}{x_7 - x_8}. \quad (7)$$

The output power of the turbine is written as

$$\dot{W}_t = \dot{m}_7(h_7 - h_9) = \dot{m}_7(h_7 - h_{9s})\eta_t. \quad (8)$$

The expansion through the expansion valve is modelled as an isenthalpic throttling process, so

$$h_8 = h_{10}. \quad (9)$$

The mixing process in Mixer 1 can be represented by

$$\dot{m}_{11} x_{11} = \dot{m}_9 x_9 + \dot{m}_{10} x_{10}, \quad (10)$$
$$\dot{m}_{11} = \dot{m}_9 + \dot{m}_{10}, \quad (11)$$
$$\dot{m}_{11} h_{11} = \dot{m}_9 h_9 + \dot{m}_{10} h_{10}. \quad (12)$$

Similar to Separator 1, the mathematical model of Separator 2 is expressed as

$$\dot{m}_{12} x_{12} = \dot{m}_{13} x_{13} + \dot{m}_{14} x_{14}, \quad (13)$$
$$\dot{m}_{12} = \dot{m}_{13} + \dot{m}_{14}, \quad (14)$$

and

$$\dot{m}_{12} h_{12} = \dot{m}_{13} h_{13} + \dot{m}_{14} h_{14}. \quad (15)$$

Accordingly, the ratio of the mass flow rate of state 13 to the total mass flow rate at state 12 is defined as

$$r_L = \frac{x_{12} - x_{14}}{x_{13} - x_{14}}. \quad (16)$$

The input power of Pump 2 is calculated by

$$\dot{W}_{p2} = \dot{m}_{16}(h_{16} - h_{15}) = \dot{m}_{16}(h_{16s} - h_{15})/\eta_p. \quad (17)$$

The mass and energy equations of Mixer 2 can be expressed as

$$\dot{m}_{17} x_{17} = \dot{m}_{13} x_{13} + \dot{m}_{16} x_{16}, \quad (18)$$
$$\dot{m}_{17} = \dot{m}_{13} + \dot{m}_{16}, \quad (19)$$

and

$$\dot{m}_{17} h_{17} = \dot{m}_{13} h_{13} + \dot{m}_{16} h_{16}. \quad (20)$$

The heat transfer in the air-cooled condenser is determined by

$$\dot{Q}_c = \dot{m}_{17}(h_{17} - h_1) = \dot{m}_{air}(h_{21} - h_{20}). \quad (21)$$

The power consumption of the fans of the air-cooled condenser is calculated by [34,35]

$$\dot{W}_c = N_f \dot{W}_{f0} \left(\frac{\dot{m}_f}{\dot{m}_{f0}}\right)^3, \quad (22)$$

where N_f is the number of the fans, $\dot{m}_f$, $\dot{m}_{f0}$ are the actual and rated fan air mass flow rates, respectively. $\dot{W}_{f0}$ is the rated fan power consumption.

The air mass flow for each fan is determined by

$$\dot{m}_f = \dot{m}_{air}/N_f. \quad (23)$$

The net power output of the Kalina cycle system is

$$\dot{W}_n = \dot{W}_t - \dot{W}_{p1} - \dot{W}_{p2} - \dot{W}_c. \quad (24)$$

The thermal efficiency of the Kalina cycle is defined as

$$\eta_{th} = \dot{W}_n / \dot{Q}_e. \quad (25)$$

Exergy analysis is based on the second law of thermodynamics to estimate the irreversibility of a process. In this model, only the physical exergy is taken into account, while the chemical exergy for steady flowing fluid is neglected. The exergy of a steady state can be defined as

$$\dot{E}_i = \dot{m}_i[(h_i - h_0) - T_0(s_i - s_0)], \quad (26)$$

where the subscript 0 denotes the ambient conditions. Similar to the energy equation, the exergy equation can be expressed by

$$\dot{I}_d = \sum \dot{E}_{in} - \sum \dot{E}_{out} - \dot{W}. \quad (27)$$

Therefore, the exergy destruction rate for each component of the Kalina cycle system can be determined.

The exergy destruction rate of Pump 1 is represented by

$$\dot{I}_{p1} = \dot{E}_3 - \dot{E}_4 + \dot{W}_{p1}. \quad (28)$$

For the recuperator,

$$\dot{I}_{re} = \dot{E}_4 - \dot{E}_5 + \dot{E}_{11} - \dot{E}_{12}. \quad (29)$$

For the evaporator,

$$\dot{I}_e = \dot{E}_5 - \dot{E}_6 + \dot{E}_{18} - \dot{E}_{19}. \quad (30)$$

For Separator 1,

$$\dot{I}_{s1} = \dot{E}_6 - \dot{E}_7 - \dot{E}_8. \quad (31)$$

For the turbine,

$$\dot{I}_t = \dot{E}_7 - \dot{E}_9 - \dot{W}_t. \quad (32)$$

For the expansion valve,

$$\dot{I}_v = \dot{E}_8 - \dot{E}_{10}. \quad (33)$$

For Mixer 1,

$$\dot{I}_{m1} = \dot{E}_9 + \dot{E}_{10} - \dot{E}_{11}. \quad (34)$$

For Separator 2,

$$\dot{I}_{s2} = \dot{E}_{12} - \dot{E}_{13} - \dot{E}_{14}. \quad (35)$$

For Pump 2,

$$\dot{I}_{p2} = \dot{E}_{15} - \dot{E}_{16} + \dot{W}_{p2}. \quad (36)$$

For Mixer 2,

$$\dot{I}_{m2} = \dot{E}_{13} + \dot{E}_{16} - \dot{E}_{17}. \quad (37)$$

For the air-cooled condenser, assuming all the heat transfer to the air is discharged to the environment, the exergy destruction rate is calculated by

$$\dot{I}_c = \dot{E}_{17} - \dot{E}_1 + \dot{W}_c. \quad (38)$$

The overall exergy destruction rate of the Kalina cycle is determined as

$$\dot{I}_{tot} = \sum \dot{I}_i = \dot{E}_{18} - \dot{E}_{19} + \dot{W}_{p1} + \dot{W}_{p2} + \dot{W}_c - \dot{W}_t. \quad (39)$$

Therefore, the exergy efficiency of the Kalina cycle is

$$\eta_{ex,cyc} = \frac{\dot{W}_n}{\dot{E}_{18} - \dot{E}_{19}}. \quad (40)$$

In this study, some assumptions are made as follows: all the working processes are steady; the pressures at all the states during the operation are constant; the thermodynamic properties at states 1, 2, and 3 are the same; the states 14 and 15 are the same. In addition, the turbine is assumed to operate with a constant isentropic efficiency across the range of mass flow rates presented to it, and this assumption is believed to be feasible [36]. That allows us to apply the model to analyse the cycle performance when the mass flow rates of the turbine varies as the ambient temperature changes from one season to another. The present research assumed that the brine from a geothermal production borehole has a fixed flow rate and temperature, and thus the design target is to maximise the power production.

Table 1
Input parameters of the composition-adjustable Kalina cycle system.

Item	Parameter	Values
Heat source	Temperature T_{18}	120 °C
	Mass flow rate $\dot{m}_{water}$	141.8 kg/s
	Pressure P_{18}	2 MPa
Evaporator	Minimal pinch $\Delta T_{e,PPTD}$	5 K
	Maximum output temperature T_6	107.3 °C
	Maximum output pressure P_6	2.28 MPa
	Pressure drop (HT side) $\Delta P_{e,h}/P_{18}$	1.95%
	Pressure drop (LT side) $\Delta P_{e,l}/P_5$	1.94%
Recuperator	Minimal pinch $\Delta T_{re,PPTD}$	5 K
	Pressure drop (HT side) $\Delta P_{re,h}/P_{11}$	0.63%
	Pressure drop (LT side) $\Delta P_{re,l}/P_4$	2.8%
Condenser	Minimal pinch $\Delta T_{c,PPTD}$	10 K
	Pressure drop (HT side) $\Delta P_{c,h}/P_{17}$	1.93%
	Number of fans	40
	Power of fan	34 kW
	Air mass flow rate	120 kg/s per fan
Turbine	Isentropic efficiency η_t	0.85
Pump	Isentropic efficiency η_p	0.8

A program was developed using Matlab. In this model, the thermodynamic properties of the ammonia-water mixture need to be determined. These values are computed by Refprop 9.1 based on the Helmholtz free energy method. The uncertainties of the equation of state are 0.2% in density, 2% in heat capacity, and 0.2% in vapour pressure [37]. The performance of a conventional KSG-1 Kalina cycle was computed at first. The main input parameters are listed in Table 1. The mass flow rate of the brine is set to 141.8 kg/s, the same as that used in the patent [25]. As there are two-phase states of the ammonia-water mixture in the heat exchangers, where the temperature of the mixture glides with the heat transfer quantity, a pinch analysis method [38] is used to determine the pinch point position and the overall heat transfer.

In order to verify the model, the computed results are compared with some published data [25] as listed in Table 2. The absolute errors of the heat transfer for all the heat exchangers are less than 1.6%, verifying the computing program developed in this research.

4. Simulation of a Kalina cycle with composition adjustment

The verified program is then used to analyse the performance of the tested composition-adjustable Kalina cycles. The air temperature data of Beijing in 2015 shown in Fig. 5 are used as the ambient conditions for this analysis. The cycle is optimised according to the average air temperature of each month. The flow chart for the optimisation algorithm is shown in Fig. 6. Firstly, the temperature and mass flow rate of the brine are specified. The temperature and pressure of state 6 are then set. Next, the pressures at all other states are determined based on the pressure drops. Then, the minimum temperature of the ammonia-water mixture at state 1 is calculated according to the ambient temperature and the pinch point temperature difference. The minimum mass fraction of ammonia in the basic solution corresponding to P_1 and T_1 is computed. Based on the mathematical model, the working process for each component of the Kalina cycle system is computed. Both the thermal and

Table 2
Model validation with the results of Lengert [25].

State	T/°C		P/MPa		h/kJ kg^{-1}		$\dot{m}$/kg s^{-1}	
	Our results	Lengert	Our results	Lengert	Our results	Lengert	Our results	Lengert
7	107.3	106.7	2.28	2.23	1823.4	1507.8	27.339	27.59
9	55.52	56.51	0.6664	0.7158	1663.3	1355.9	27.339	27.59
3	13.62	13.13	0.651	0.69	353.8	24.8	28.104	27.6
5	51.66	53.52	2.392	2.326	539.3	221.4	28.104	27.6
18	120	119.9	2	2	505.08	−1997.8	141.8	141.8
19	61.29	57.45	1.961	1.961	258.22	−2250.6	141.8	141.8

Heat exchanger	Power/kW	
	Our results	Lengert
Evaporator	35.01	34.5
Recuperator	5.22	5.3
Condenser	31.27	31

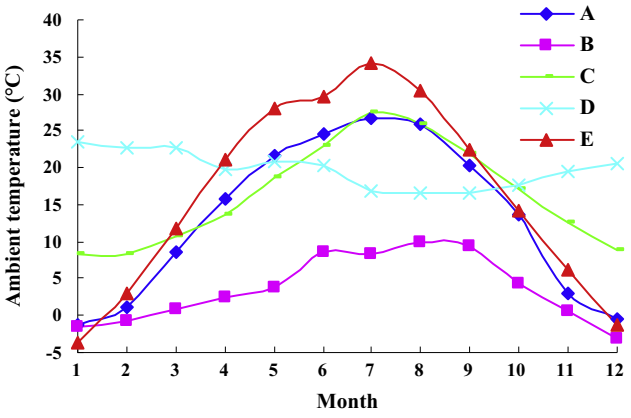

Fig. 5. Average monthly temperature profiles for different regions: A–Beijing (China); B–Husavik (Iceland); C–Rome (Italy); D–Lima (Peru); E–Turpan (China).

exergy efficiencies are then determined. An iterative algorithm is used to compute the heat transfer within the recuperator, the evaporator, and the condenser according to a predefined pinch point temperature difference. In addition, according to the working pressures of Separators 1 and 2, the corresponding bubble and dew lines are determined. Consequently, the ammonia mass fractions at the outlets of the separators can be obtained based on the Lever rule of zeotropic mixtures [39].

In this research, in order to study the effect of composition adjustment on the system's performance, a conventional KSG-1 Kalina cycle represented by Cycle B was also simulated. The results are compared with the composition-adjustable Kalina cycle denoted as Cycle A.

In Cycle A, the composition of its ammonia-water mixture can be adjusted according to the ambient temperature. As a benchmark, Cycle B, a conventional Kalina cycle, has a fixed composition of the working fluid mixture, and thus a fixed condensing temperature. To allow Cycle B to operate over a year when the ambient temperature fluctuates from the minimum in winter to the maximum in summer, it has to be designed based on the maximum ambient temperature in a year. For this reason, the maximum temperature over a year was selected to model Cycle B. As a result, it will have a constant thermal efficiency throughout a year.

5. Results analysis

5.1. Effect of composition tuning

Based on the developed numerical model, an optimisation procedure as shown in Fig. 6 was used to analyse the effect of adjusting ammonia mass fraction in the basic solution on the performance of Cycle A. The ambient temperature in October at 13.76 °C was used as a sample case. Figs. 7–9 show the system's performance as a function of the ammonia mass fraction in the basic solution x_b. The mass flow rate of the basic solution is given in Fig. 7(a). It decreases from 57.69 kg/s to 31.67 kg/s as x_b increases from 0.502 to 0.792. This can be attributed to that the evaporated mass flow of the basic solution increases with the increase of x_b, but the heat transfer of the brine in the evaporator cannot increase proportionally. The temperatures at the inlet and outlet of the recuperator are shown in Fig. 7(b). The temperature at the inlet of Pump 1 decreases with the increase of x_b due to a constant pressure at the inlet of Pump 1. The temperature difference at the inlet and outlet of the recuperator is small. The temperature at the outlet of the high temperature side of the recuperator has a similar tendency because the temperature at the inlet of the high temperature side decreases. The temperatures of the brine at the inlet and outlet of the evaporator are shown in Fig. 7(c). For the convenience of comparing the results with some published data, the inlet temperature of the brine is fixed at 120 °C. The temperature of the brine at the outlet of the evaporator decreases gradually because the basic solution becomes easier to evaporate as x_b increases, and thus the heat transfer in the evaporator also increases.

Fig. 7(d) shows the temperatures in the turbine and Mixer 1. The temperature at the inlet of the turbine remains 107.3 °C, the same as the outlet of the evaporator. Because the temperature, the pressure, and the ammonia mass fraction of the work solution at the inlet of the turbine remain constant when x_b increases, the temperature at the outlet of the turbine remains constant accordingly. The temperature of the ammonia-lean solution at the outlet of the expansion valve also remains constant. However, after these two streams are mixed in Mixer 1, the temperature at the outlet of Mixer 1 decreases gradually as x_b increases.

The mass flow rates at the outlet of Separator 1 are given in Fig. 8(a). As x_b increases, the mass flow rate of the ammonia-rich work solution increases, but the mass flow rate of the ammonia-lean solution decreases. The mass flow rates at the outlet of Separator 2 are shown in Fig. 8(b), and they have similar tendencies to those shown in Fig. 8(a). As shown in Fig. 8(c), both the temperatures of the basic solution at the inlet and outlet of the condenser decrease as x_b increases. It can be seen in Fig. 8(d), the mass flow rate of air increases significantly as x_b increases. Accordingly, the air temperature at the outlet of the condenser drops gradually.

The power consumption of each component is shown in Fig. 9 (a). When the ammonia fraction x_b increases, the power consumption of both Pumps 1 and 2 decreases gradually because the

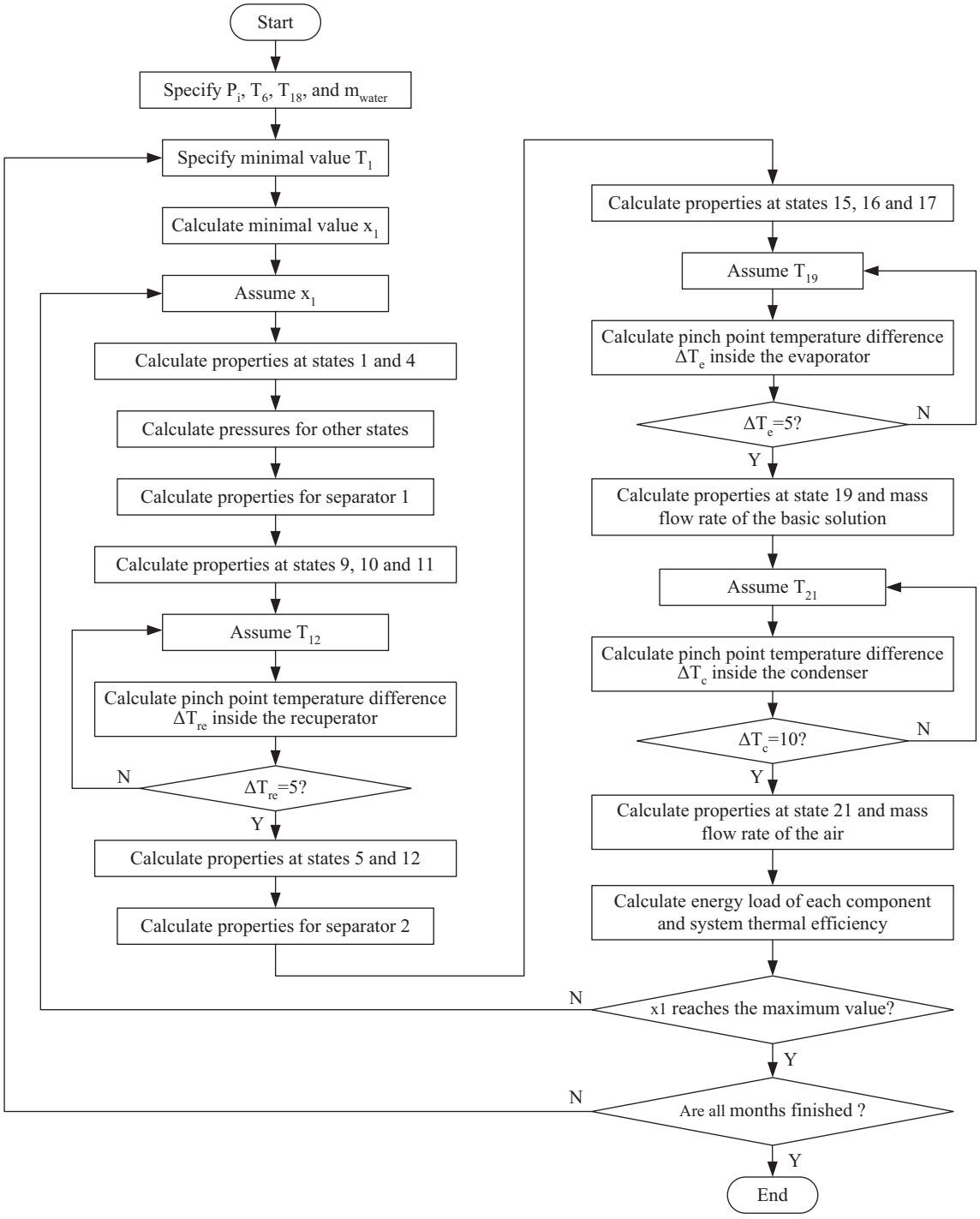

Fig. 6. Flow chart of the optimisation process.

enthalpy of the solution decreases with the increase of x_b if the outlet pressures of the pumps are kept constant. The power consumption of the fans increases rapidly because the mass flow rate of the air rises significantly as x_b increases. The heat transfer rates within the evaporator and the condenser are shown in Fig. 9(b). Both of them increase evidently as x_b increases. When x_b is 0.502, the heat transfer rate of the evaporator and the condenser is 19.15 MW and 18.35 MW, respectively. However, when x_b further increases to 0.792, they increase to 29.12 MW and 26.19 MW, respectively. The power output of the turbine and the net power output of the cycle are presented in Fig. 9(c). The total power consumption of the pumps and the condenser fans is also shown in this figure. The power output of the turbine rises as x_b increases due to the increase of the mass flow rate of the work solution. The total power consumption also increases as x_b increases, and it increases significantly when x_b is above 0.79. As a result, the net power output firstly increases and then decreases. The maximum net power output occurs when x_b is around 0.782.

The cycle's thermal and exergy efficiencies are shown in Fig. 9(d). Both of them firstly increase and then decrease when x_b increases from 0.502 to 0.792. The maximum thermal efficiency and exergy efficiency occur when x_b is around 0.762 and 0.772, respectively. The ammonia mass fractions corresponding to the maximum points of the thermal and the exergy efficiencies are very close.

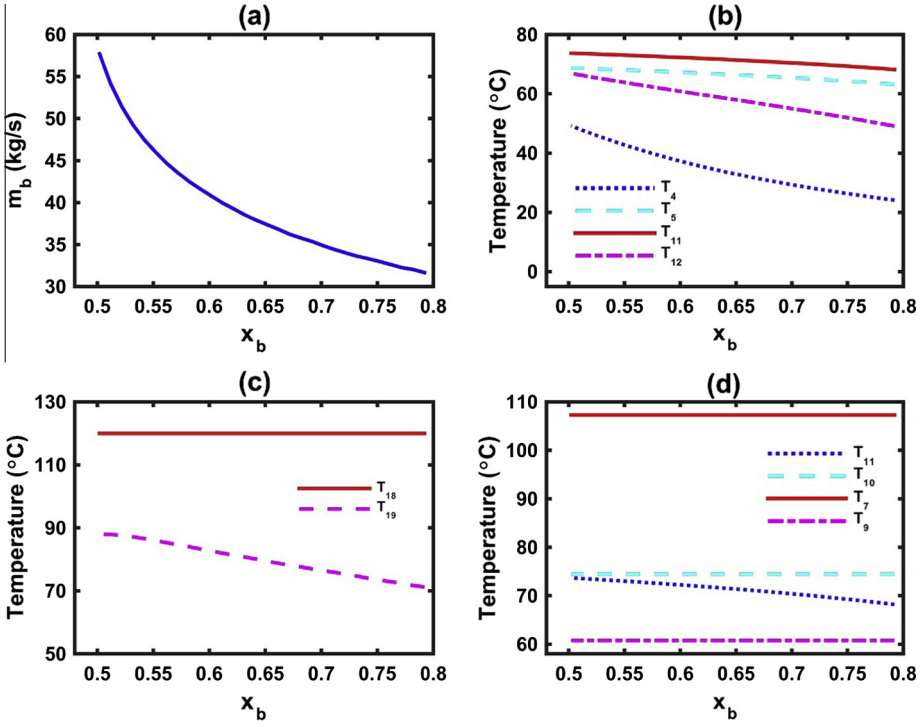

Fig. 7. Results of the mass flow rate and temperatures under the annual average ambient temperature: (a) mass flow rate of the basic solution; (b) temperatures at the inlet and outlet of the recuperator; (c) temperature of the geothermal brine; (d) temperatures at the inlet and outlet of the turbine and Mixer 1.

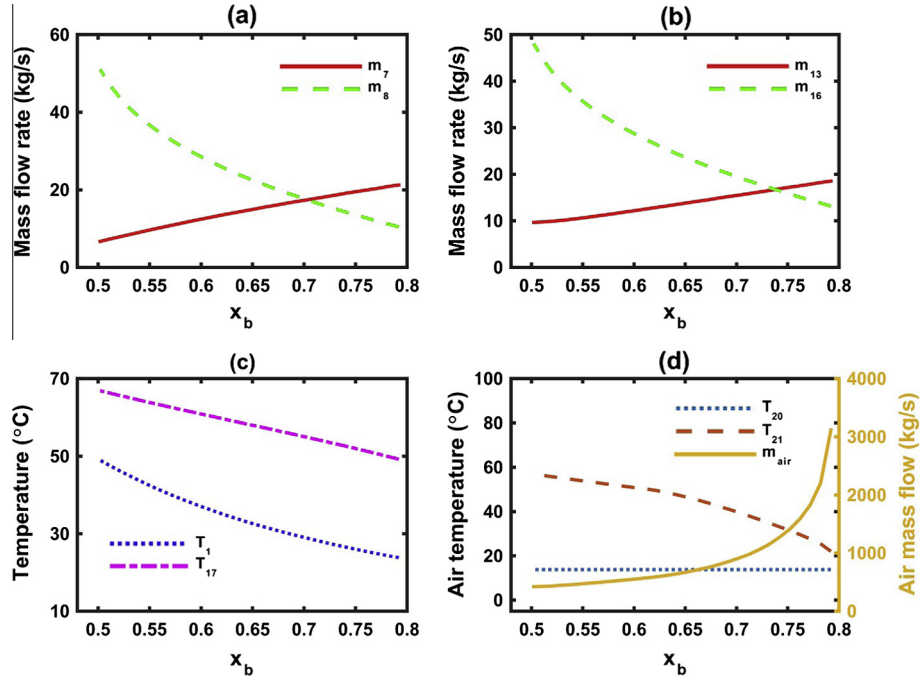

Fig. 8. Performance of the components under the annual average ambient temperature: (a) mass flow rates at the outlets of Separator 1; (b) mass flow rates at the outlets of Separator 2; (c) temperatures of the basic solution at the inlet and outlet of the condenser; (d) mass flow rate and temperatures of the air flow in the condenser.

5.2. Performance comparison with conventional Kalina cycle

The efficiencies of Cycles A and B defined in Section 4 were then computed according to the monthly average temperature throughout a year in Beijing. Cycle A is designed to match the ambient air temperature during a year. In spring or autumn, the ambient temperature is moderate, and it is represented as T_{a1} in Fig. 10. The temperature of the liquid ammonia-water mixture at the outlet of the condenser (i.e., state 1 in Fig. 2.) is denoted as Point A in Fig. 10. The temperature difference between state 1 and the ambient ΔT is constrained by the pinch point temperature difference. When the season shifts to winter, the ambient temperature decreases from T_{a1} to T_{a2}. State 1 moves from Point A to Point B. During this shifting process, only the ammonia mass fraction is

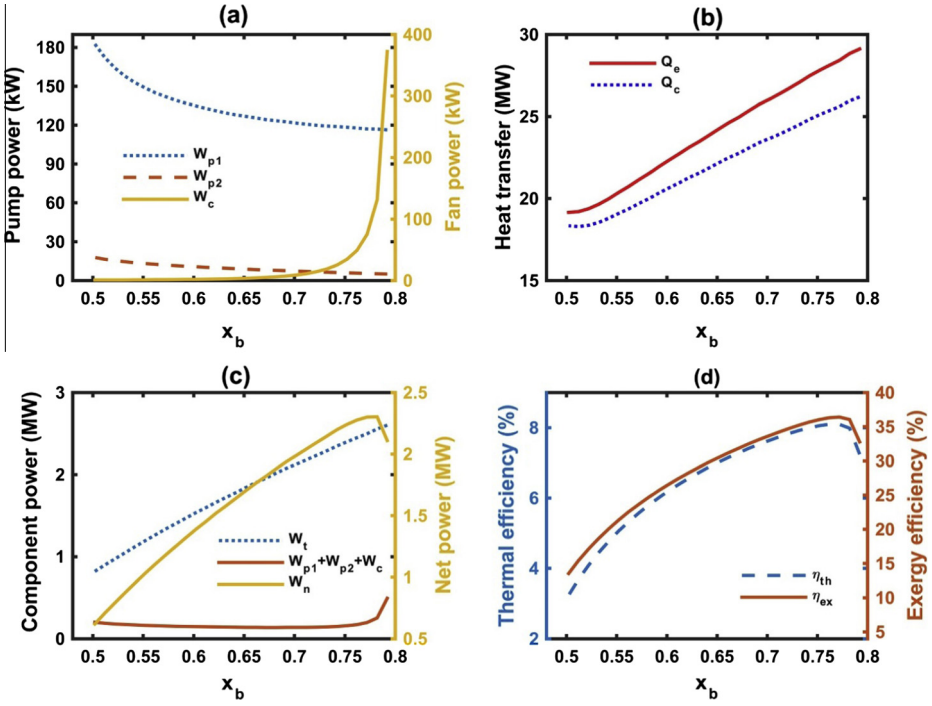

Fig. 9. System performance at the annual average ambient temperature: (a) power consumption of Pumps 1 and 2 and the fans; (b) heat transfer rates of the evaporator and the condenser; (c) Net power output of the Kalina cycle and power output of the turbine; (d) thermal and exergy efficiencies of the cycle.

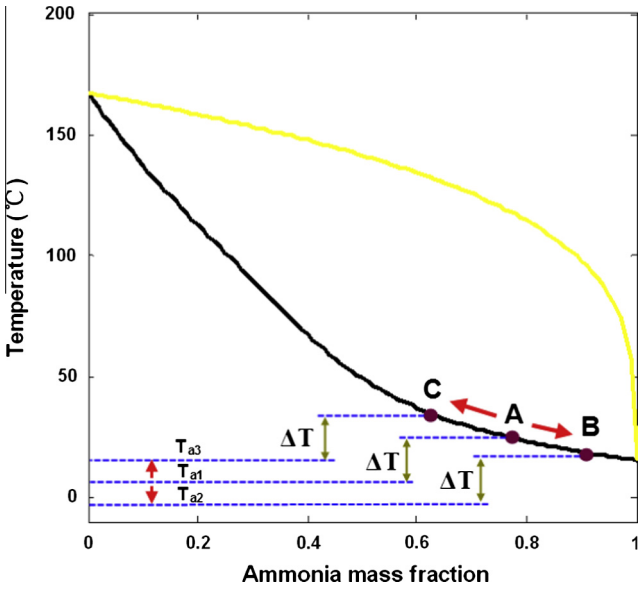

Fig. 10. Composition adjustment process of the ammonia mass fraction of the basic solution.

adjusted, while the condensation pressure of the ammonia-water mixture is kept as constant. If the season shifts to summer, state 1 will move from Point A to Point C according to the increase of ambient temperature from T_{a1} to T_{a3}. Under these conditions, the condensation pressure of Cycle B is the same as Cycle A. The temperature at state 1 of Cycle B must be determined based on the maximum month-average temperature over a year.

The thermal efficiency of Cycle A as a function of both x_b and the ambient temperature is shown in Fig. 11(a). It can be seen that the ambient temperature has a strong effect on the cycle thermal efficiency. For a given value of x_b, the thermal efficiency increases as the ambient temperature decreases. Fig. 11(b) gives the corresponding results of the thermal efficiency against x_b for each month. The solid line represents the thermal efficiency for each month, while the dashed line represents the optimal operation line (OOL), i.e., maximum thermal efficiency. It can be seen that for each month the thermal efficiency first increases then decreases as x_b increases. This is because the power output of the turbine increases as x_b increases, but the power consumption of the cooling fans of the condenser increases too, especially when x_b is high. The optimised x_b based on the thermal efficiency is in the range of 0.603–0.95, and the corresponding thermal efficiency is in the range of 6.12–9.24%.

Fig. 11(c) shows the thermal efficiency of Cycles A and B as a function of ambient temperature. The results of Cycle A corresponding to the optimal operation line of the thermal efficiency are shown in Fig. 11(a). The thermal efficiency of Cycle B is constant at 6.12%. However, the thermal efficiency of Cycle A increases from 6.12% to 9.24% because, as the ambient temperature decreases, the power output of the turbine increases significantly by matching the condensation temperature of ammonia-water mixture with the ambient air temperature.

Fig. 11(d) shows the calculated exergy efficiency of Cycle A as a function of both x_b and ambient temperature. The variation of the exergy efficiency has a similar tendency to that of the thermal efficiency as shown in Fig. 11(e). The heat source of the 2 MW Kalina power plant in Husavik is a low-temperature geothermal brine at 120 °C, and its x_b of the Kalina cycle is 0.82. This case is denoted as a red[1] line in Fig. 11(b) and (d), and it is close to the optimal results at the ambient temperature of 2.94 °C according to the present simulation. It should be noted that, in this research, an air-cooled condenser is used instead, and its pinch point temperature difference is greater than that of a water-cooled condenser. There-

[1] For interpretation of color in Fig. 11, the reader is referred to the web version of this article.

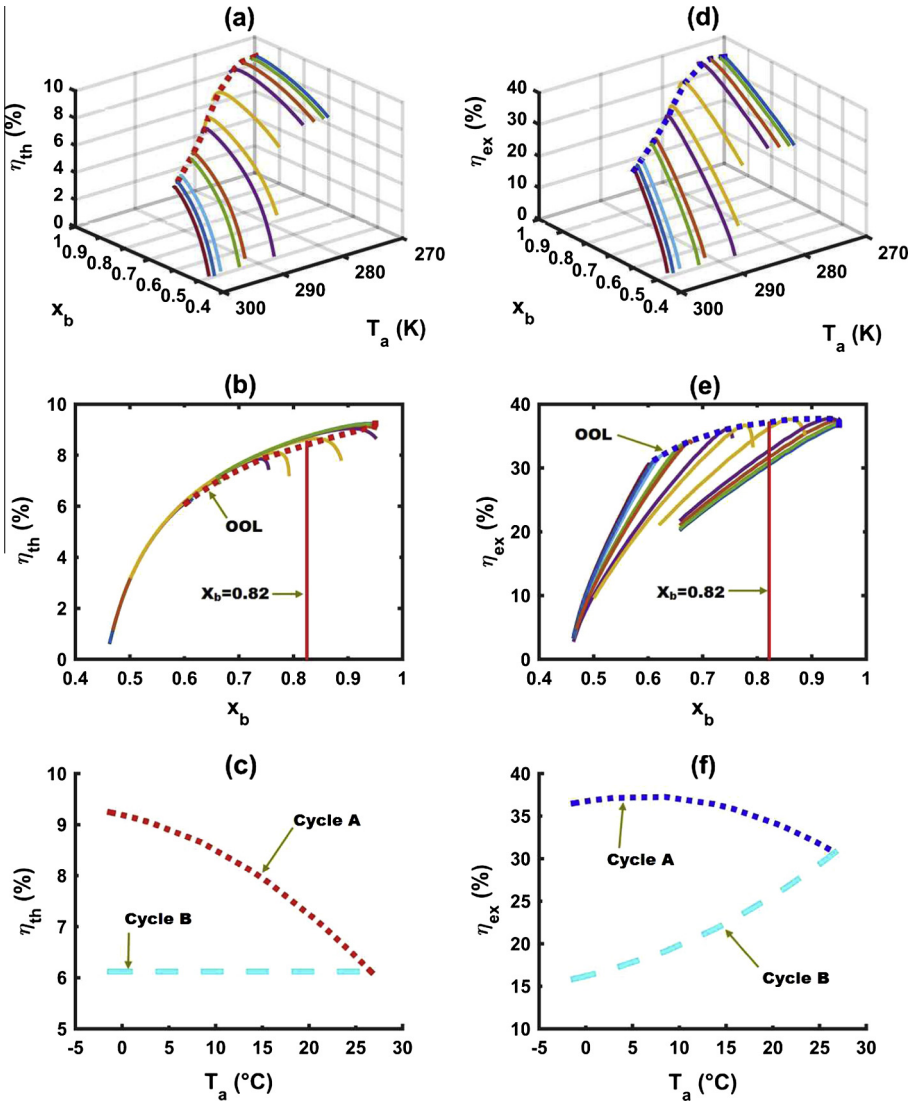

Fig. 11. Optimised results of the composition-adjustable Kalina cycle system as a function of the ambient temperature: (a) the thermal efficiency surface; (b) the thermal efficiency as a function of x_b; (c) comparison of the thermal efficiency between the two cycles; (d) the exergy efficiency surface; (e) the exergy efficiency as a function of x_b; (c) comparison of exergy efficiency between the two cycles.

fore, the corresponding ambient temperature is about 2 °C less than that of the Husavik's geothermal power plant.

The exergy efficiencies of Cycles A and B are given in Fig. 11(f). The exergy efficiency of Cycle A increases from 30.7 to 36.5% as the ambient temperature decreases from 26.6 to −1.3 °C. In contrast, the exergy efficiency of Cycle B decreases from 30.7 to 16.5% because the net power output of Cycle B is constant while the exergy of the brine increases as the ambient temperature decreases.

5.3. Optimal results based on thermal efficiency

In this section, we assume the system operates along the optimal operation line of the cycle's thermal efficiency (see Fig. 11(a)). In this case, the mass flow rate of the geothermal brine is fixed as 141.8 kg/s. The net power outputs corresponding to the maximum thermal efficiency are given in Fig. 12(a). The net power output increases significantly with the decrease of the ambient temperature. The average ambient temperature of Beijing in July reaches a maximum of 26.6 °C, and the corresponding net power output is 1.366 MW. In contrast, the lowest temperature is −1.3 °C in January, and the net power output is 3.145 MW, which is 2.3 times of that in July. This demonstrates the benefit of matching the cycle with ambient conditions by adjusting the composition of the mixture. The corresponding thermal efficiency and exergy efficiencies are shown in Fig. 12(b). As the ambient temperature decreases from the maximum (26.6 °C) to the minimum (−1.3 °C), the thermal efficiency increases from 6.12% to 9.24%. Accordingly, the exergy efficiency increases from 30.7 to 36.5%. Fig. 12(c) shows the optimised x_b as a function of the ambient temperature, which increases as the ambient temperature decreases. As shown in Fig. 12(d), the corresponding density of the ammonia-water mixture decreases from 780 kg/m^3 to 640 kg/m^3 as the ambient temperature drops. Density sensors having an accuracy of ±0.1 kg/m^3 are widely available in the market, which is sufficient for the real-time control of the ammonia mass fraction as required by the system modelled in this paper.

Fig. 13(a) shows the power consumption of the pumps and the condenser fans. The power consumption of Pump 1 is of the same order as the fans, while the power consumption of Pump 2 is much less than them. As the ambient temperature decreases, the power of Pump 1 decreases from 134 kW to 114 kW, while

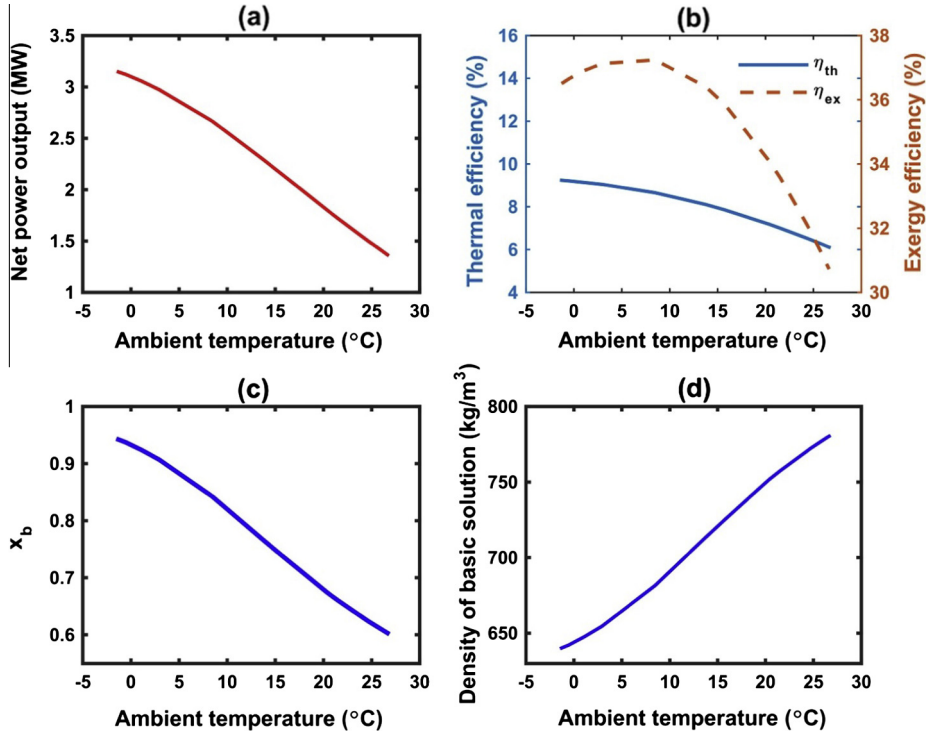

Fig. 12. Results on the optimal operation line of the thermal efficiency: (a) the net power output; (b) the system thermal efficiency and the exergy efficiency; (c) the ammonia mass fraction of the basic solution; (d) the density of the basic solution.

the power consumption of the fans firstly increases and then decreases slightly. The power output of the turbine and the net power output of the cycle are shown in Fig. 13(b). Since the power output of the turbine is far greater than the total power consumed, the tendency of the net power output is similar to that of the power output of the turbine. The mass flow rates of the basic solution and the cooling air are shown in Fig. 13(c). As the ambient temperature drops, the mass flow rate of the basic solution decreases but the mass flow of the air increases. The mass ratios in the two separators are also given in Fig. 13 (d). The mass ratio of Separator 2 is lower than that of Separator 1 because the operation temperature of Separator 1 is higher than that of Separator 2.

Fig. 13(e) shows the heat transfer between the geothermal brine and the ammonia-water mixture in the evaporator. As the ambient temperature decreases from 26.6 °C to −1.3 °C, the heat transfer increases from 22.34 MW to 34.03 MW. The temperature of the brine at the outlet of the evaporator is also given in this figure, and it decreases as the ambient temperature decreases. The heat transfer within the evaporator increases evidently due to the temperature drop at the inlet of the low-temperature side. As shown in Fig. 13(f), the heat transfer of the condenser increases as the ambient temperature decreases. It can be seen that the air temperature at the outlet of the condenser decreases as the ambient temperature decreases.

From the viewpoint of thermal efficiency, the benefits of matching the condensing temperature to the ambient condition via composition adjustment are further analysed and summarised in Table 3. It should be noted that Cycle A operates along the OOL of thermal efficiency. However, for Cycle B, x_b and T_1 are fixed as 0.603 and 36.6 °C, respectively, according to the ambient temperature in July. The annual average values of the net power output, the heat transfer of the evaporator, and the thermal efficiency are calculated using Eqs. (41), (42), and (43), respectively.

$$\overline{W}_n = \frac{1}{N}\sum_{i=1}^{N}\dot{W}_n(i) \tag{41}$$

$$\overline{Q}_e = \frac{1}{N}\sum_{i=1}^{N}\dot{Q}_e(i) \tag{42}$$

$$\bar{\eta}_{th} = \frac{1}{N}\sum_{i=1}^{N}\eta_{th}(i) \tag{43}$$

Here N is the total months of a year. The annual average improvement of Cycles A relative to Cycle B is determined by Eqs. (44) to (46), respectively.

$$\psi_W = \frac{\overline{W}_{n,A} - \overline{W}_{n,B}}{\overline{W}_{n,B}} \times 100\% \tag{44}$$

$$\psi_Q = \frac{\overline{Q}_{e,A} - \overline{Q}_{e,B}}{\overline{Q}_{e,B}} \times 100\% \tag{45}$$

$$\psi_\eta = \frac{\bar{\eta}_{th,A} - \bar{\eta}_{th,B}}{\bar{\eta}_{th,B}} \times 100\% \tag{46}$$

The annual average thermal efficiency of Cycle A is 7.86%, and it is about 28.39% higher than that of Cycle B at 6.12%. On the other hand, the annual average heat transfer of the evaporator of Cycle A is also 26.23% higher than that of Cycle B. As a result, the annual average net power output of Cycles A and B is 2.267 and 1.366 MW, respectively. The former is 65.99% higher than the latter.

The computed results of the Kalina cycle based on the annual average air temperature of Beijing are listed in Table 4. The thermal efficiency is 8.10% and the exergy efficiency is 24.27%. The corresponding exergy destruction rate for each component is shown in Fig. 14. The condenser causes the largest exergy destruction rate at 1726 kW, followed by the evaporator

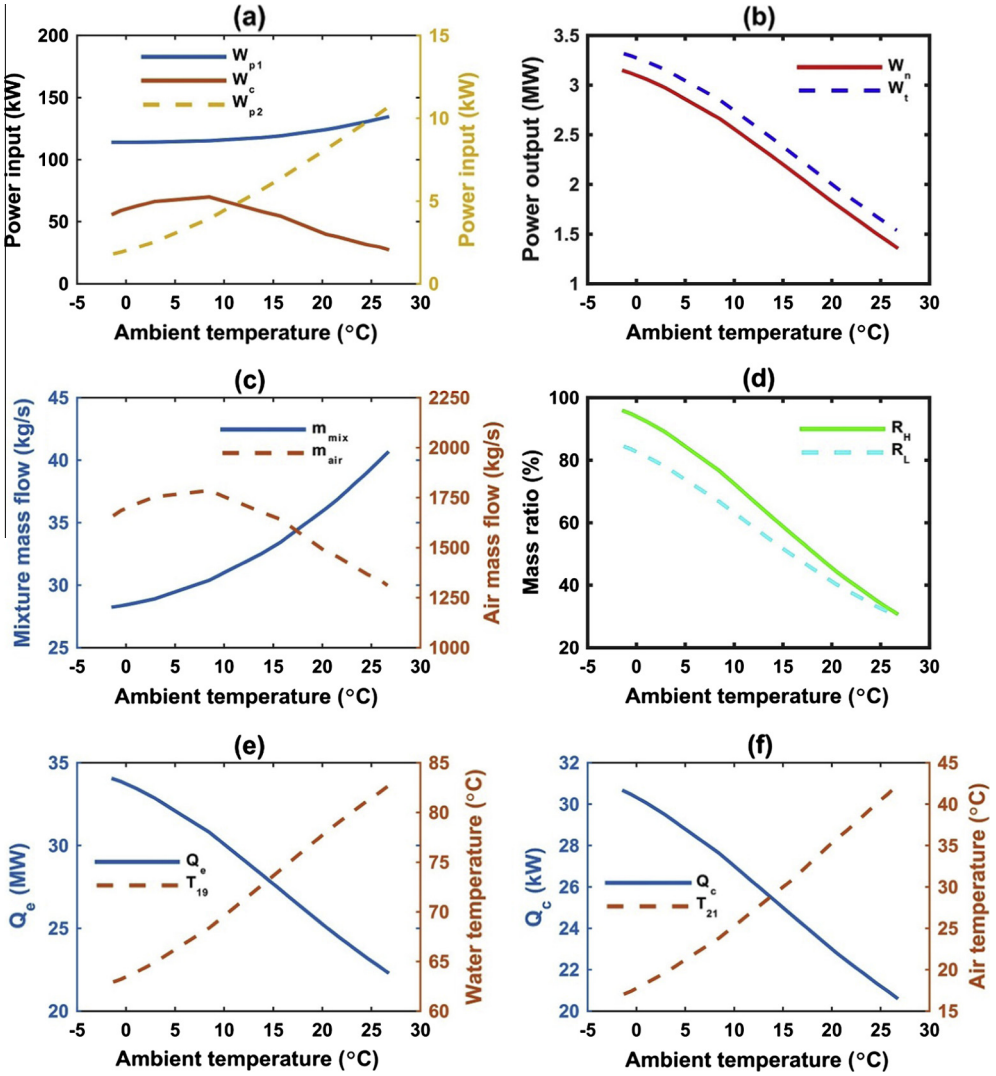

Fig. 13. Performance of the components as a function of the ambient temperature: (a) power consumption by Pumps 1, 2, and the condenser; (b) the turbine power output and the system net power output; (c) the mass flow rates of the ammonia-water mixture and the air; (d) the mass ratios of Separators 1 and 2; (e) the mass flow rate of the brine and the water temperature at the outlet; (f) the heat transfer of the condenser and the air temperature at the outlet.

Table 3
Performance comparison between the two cycles.

Month	Cycle A			Cycle B			Improvement		
	Wn/MW	Qe/MW	η_{th}/%	Wn/MW	Qe/MW	η_{th}/%	ψ_W	ψ_Q	ψ_η
1	3.145	34.03	9.24	1.366	22.34	6.12	130.23	52.31	50.98
2	3.057	33.44	9.14	1.366	22.34	6.12	123.79	49.65	49.35
3	2.665	30.80	8.65	1.366	22.34	6.12	95.10	37.86	41.34
4	2.146	27.32	7.85	1.366	22.34	6.12	57.10	22.28	28.27
5	1.718	24.54	7.00	1.366	22.34	6.12	25.77	9.82	14.38
6	1.501	23.18	6.48	1.366	22.34	6.12	9.88	3.74	5.88
7	1.366	22.34	6.12	1.366	22.34	6.12	0.00	0.00	0.00
8	1.425	22.72	6.27	1.366	22.34	6.12	4.32	1.67	2.45
9	1.800	25.06	7.18	1.366	22.34	6.12	31.77	12.17	17.32
10	2.293	28.29	8.10	1.366	22.34	6.12	67.86	26.60	32.35
11	2.973	32.87	9.05	1.366	22.34	6.12	117.64	47.08	47.88
12	3.120	33.87	9.21	1.366	22.34	6.12	128.40	51.58	50.49
Annual average	2.267	28.21	7.86	1.366	22.34	6.12	65.99	26.23	28.39

Cycle A: Kalina cycle with composition adjustment.
Cycle B: Conventional Kalina cycle without any regulation.

(916 kW) and the turbine (881 kW). If the irreversibility loss of the condenser can be reduced further, the system performance can be further improved.

The potential of performance improvement for different climate conditions are also evaluated. In addition to Beijing, four other locations are considered, including Lima (Peru); Husavik (Iceland),

Table 4
Thermodynamic properties of the composition-adjustable Kalina cycle system operating at the annual average ambient temperature of Beijing.

State	T/°C	P/MPa	h/kJ kg^{-1}	s/kJ kg^{-1}K^{-1}	$\dot{m}$/kg s^{-1}	x/%	Quality
1	25.14	0.738	217.61	1.399	32.505	0.766	0
2	25.14	0.738	217.61	1.399	32.505	0.766	0
3	25.14	0.738	217.61	1.399	32.505	0.766	0
4	25.48	2.392	220.50	1.401	32.505	0.766	0
5	63.89	2.325	416.70	2.019	32.505	0.766	0
6	107.3	2.28	1287.0	4.476	32.505	0.766	0.621
7	107.3	2.28	1823.4	6.005	20.184	0.964	1
8	107.3	2.28	408.38	1.970	12.321	0.441	0
9	60.76	0.760	1679.2	6.082	20.184	0.964	0.957
10	74.45	0.760	408.40	2.007	12.321	0.441	0.117
11	68.88	0.760	1197.5	4.539	32.505	0.766	0.633
12	50.88	0.753	1001.3	3.952	32.505	0.766	0.544
13	50.88	0.753	1717.6	6.214	17.687	0.994	1
14	50.88	0.753	146.25	1.252	14.818	0.494	0
15	50.88	0.753	146.25	1.252	14.818	0.494	0
16	50.91	0.953	146.56	1.252	14.818	0.494	0
17	50.95	0.753	1002.2	3.955	32.505	0.766	0.544
18	120	2	505.08	1.526	141.8	–	–
19	72.61	1.961	305.58	0.986	141.8	–	–
20	13.76	0.118	287.09	6.778	1679.0	–	–
21	28.83	0.113	302.28	6.842	1679.0	–	–

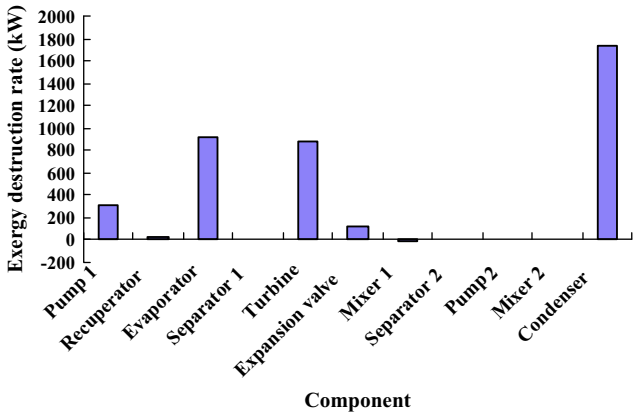

Fig. 14. The exergy destruction rates of the components when the system operates at the annual average ambient temperature.

Table 5
Thermodynamic performance comparison for different locations.

Location	T_{max}/°C	T_{min}/°C	T_{mean}/°C	T_{dif}/°C	ψ_W/%	ψ_Q/%	ψ_η/%
Lima	23.4	16.5	19.8	6.9	16.58	7.11	8.61
Husavik	9.8	−3.2	3.5	13	13.09	7.50	5.06
Rome	27.6	8.3	16.4	19.3	61.09	23.22	28.93
Beijing	26.6	−1.3	13.3	27.9	65.99	26.23	28.39
Turpan	34.1	−3.7	16.3	37.8	154.02	38.08	76.11

Rome (Italy), and Turpan (China). Their monthly average ambient temperatures in 2015 are shown in Fig. 5 [40]. The maximum and minimum monthly averaged temperatures (T_{max} and T_{min}), the annual mean temperature (T_{mean}), and the annual temperature variation ($T_{dif} = T_{max} - T_{min}$) are also listed in Table 5. Based on Eqs. (44)–(46), the calculated results of the five selected locations are shown in Table 5. The annual average improvement of the thermal efficiency is nearly proportional to the annual temperature variation. The larger the annual temperature variation, the higher the annual average improvement. Furthermore, the annual mean temperature also affects the performance improvement. A lower annual mean temperature leads to a higher thermal efficiency of Cycle B. For example, the improvement of thermal efficiency of Husavik is slightly less than that of Lima.

6. Discussion

In a composition-adjustable Kalina cycle, there exists an optimal ammonia mass fraction of the basic solution for a given ambient temperature, leading to a maximum thermal efficiency. Below the optimal value, the mass flow rate of the working solution decreases as the ammonia mass fraction decreases, leading to lower power output from the turbine. Above this optimal value, the power consumption of the fans of the condenser increases significantly as the ammonia mass fraction increases, reducing the power output too.

The composition-adjustable Kalina cycle can change the ammonia mass fraction of the basic solution in response to ambient temperature so that the condensation temperature of the ammonia-water mixture can be regulated to match the changing ambient temperature. When the ambient temperature rises, the system reduces the ammonia mass fraction, so the condensation temperature of the mixture increases. When the ambient temperature drops, the system enriches the concentration of ammonia, reducing the condensation temperature. During the operation, the condensation pressure is maintained constant.

According to the analysis above, a composition-adjustable Kalina cycle can achieve a higher annual-average thermal efficiency than a conventional Kalina cycle operating on a fixed composition (ultimately a fixed condensing temperature). For a typical continental climate (e.g., Beijing), the calculated annual-average thermal efficiency can be improved significantly, the heat addition within the evaporator can also be increased accordingly. As a result, the annual net power production can be increased significantly.

However, such an improvement of the thermal efficiency strongly depends on the heat source temperature and annual temperature variation. For a given heat source temperature, the larger the annual temperature variation, the higher the improvement of thermal efficiency. For a given annual temperature variation (i.e., a given climate condition), the higher the heat source temperature, the less the improvement of thermal efficiency. This can be attributed to the fact that the thermal efficiency of the conventional Kalina cycle (Cycle B) increases as the heat source temperature increases (see Eq. (46)). For high temperature heat sources, the cycle is less sensitive to the variation of condensing temperature (ultimately the heat sink temperature).

The present research assumed that the brine from a geothermal production borehole has a fixed flow rate and temperature, and thus the design target is to maximise the power production. Based on this assumption, the system power output and components sizes of a conventional Kalina cycle (Cycle B) are designed according to the highest ambient temperature in summer. On the contrary, the components sizes of a composition-adjustable Kalina cycle (Cycle A) should be specified according to the lowest ambient temperature in the winter. A composition adjustment control system needs to be added. The mass flow rate and ammonia concentration of the basic solution of the composition-adjustable Kalina cycle are then regulated according to the changing ambient temperature. In this case, the overall power output varies as the ambient temperature changes.

For the convenience of cost comparison, power output can be fixed as the same. In this case, the capital cost of a composition-adjustable Kalina cycle power plant will be slightly more than that of a conventional Kalina cycle mainly due to the introduction of a composition adjusting system that consists of a density sensor, a control unit, and a tank (see Fig. 2). There will be a

break-even point where the additional capital and operation costs can be compensated by the gain of annual-average thermal efficiency, which however strongly depends on operation conditions such as the scale of the power plant, annual temperature variation, heat source temperature, etc. Qualitatively speaking, a combination of large annual temperature variation, low heat source temperature, and large rated power output could lead to an economically viable case.

7. Conclusions

This paper presents a comprehensive numerical analysis of a composition-adjustable Kalina cycle system. An advanced numerical model taking into account the heat transfer processes within the evaporator and condenser has been developed to demonstrate and analyse the working mechanism of this cycle in detail, and it has been verified by some published data.

Air-cooled condenser has been used in this research to maximise the effect of the ambient temperature on the cycle's performance. The effect of both air temperature and flow rate on the cycle's thermal efficiency has been analysed in detail.

The obtained results are compared with a conventional Kalina cycle with fixed composition and condensing temperature, showing a significant improvement in annual-average thermal efficiency. However, such an improvement of the thermal efficiency strongly depends on the heat source temperature and annual temperature variation. For a given heat source temperature, the larger the annual temperature variation, the higher the improvement of thermal efficiency. For a given annual temperature variation, the higher the heat source temperature, the less the improvement of thermal efficiency.

Extra components and a control system are required to implement such composition-adjustable Kalina cycle, and they introduce extra costs. The additional capital and operation costs can be compensated by the improvement of annual-average thermal efficiency (i.e., more power generation). In general, a combination of large annual temperature variation, low heat source temperature, and large rated power output is preferred for a composition-adjustable Kalina cycle. In order to quantitatively identify the break-even point, a combined thermodynamic – economic model is required, and it will be studied in detail in the future.

Acknowledgements

This research is funded by Royal Society (RG130051) and EPSRC (EP/N005228/1) in the United Kingdom, and a joint programme "Royal Society–National Natural Science Foundation of China (Ref: IE150866)".

References

[1] Walmsley MRW, Walmsley TG, Atkins MJ, Kamp PJJ, Neale JR. Minimising carbon emissions and energy expended for electricity generation in New Zealand through to 2050. Appl Energy 2014;135:656–65.
[2] Tokimatsu K, Konishi S, Ishihara K, Tezuka T, Yasuoka R, Nishio M. Role of innovative technologies under the global zero emissions scenarios. Appl Energy 2016;162:1483–93.
[3] Alcaraz M, García-Gil A, Vázquez-Suñé E, Velasco V. Use rights markets for shallow geothermal energy management. Appl Energy 2016;172:34–46.
[4] Yin H, Sabau AS, Conklin JC, McFarlane J, Qualls AL. Mixtures of SF_6–CO_2 as working fluids for geothermal power plants. Appl Energy 2013;106:243–53.
[5] Clarke J, McLeskey Jr JT. Multi-objective particle swarm optimization of binary geothermal power plants. Appl Energy 2015;138:302–14.
[6] Liu Q, Shen A, Duan Y. Parametric optimization and performance analyses of geothermal organic Rankine cycles using R600a/R601a mixtures as working fluids. Appl Energy 2015;148:410–20.
[7] Igobo ON, Davies PA. Review of low-temperature vapour power cycle engines with quasi-isothermal expansion. Energy 2014;70:22–34.
[8] Singh DV, Pedersen E. A review of waste heat recovery technologies for maritime applications. Energy Convers Manage 2016;111:315–28.
[9] Kalina AI. Generation of energy. US patent 4489563; 1984.
[10] Kalina AI. Combined-cycle system with novel bottoming cycle. ASME J Eng Gas Turb Power 1984;106:737–42.
[11] DiPippo R. Second Law assessment of binary plants generating power from low-temperature geothermal fluids. Geothermics 2004;33:565–86.
[12] Gerber L, Marechal F. Environomic optimal configurations of geothermal energy conversion systems: application to the future construction of Enhanced Geothermal Systems in Switzerland. Energy 2012;45:908–23.
[13] Campos Rodriguez CE, Escobar Palacio JC, Venturini OJ, Silva Lora EE, Cobas VM, Santos DM, et al. Exergetic and economic comparison of ORC and Kalina cycle for low temperature enhanced geothermal system in Brazil. Appl Therm Eng 2013;52:109–19.
[14] Coskun A, Bolatturk A, Kanoglu M. Thermodynamic and economic analysis and optimization of power cycles for a medium temperature geothermal resource. Energy Convers Manage 2014;78:39–49.
[15] Fallah M, Mahmoudi SMS, Yari M, Ghiasi RA. Advanced exergy analysis of the Kalina cycle applied for low temperature enhanced geothermal system. Energy Convers Manage 2016;108:190–201.
[16] Cao L, Wang J, Dai Y. Thermodynamic analysis of a biomass-fired Kalina cycle with regenerative heater. Energy 2014;77:760–70.
[17] Sun F, Zhou W, Ikegami Y, Nakagami K, Su X. Energy exergy analysis and optimization of the solar-boosted Kalina cycle system 11 (KCS-11). Renew Energy 2014;66:268–79.
[18] Yu Z, Han J, Liu H, Zhao H. Theoretical study on a novel ammonia–water cogeneration system with adjustable cooling to power ratios. Appl Energy 2014;122:53–61.
[19] Wang J, Wang J, Dai Y, Zhao P. Thermodynamic analysis and optimization of a flash-binary geothermal power generation system. Geothermics 2015;55:69–77.
[20] Hettiarachchi HDM, Golubovic M, Worek WM, Ikegami Y. The performance of the Kalina cycle system 11 (KCS-11) with low-temperature heat sources. ASME J Energy Resour Technol 2007;129:243–7.
[21] Kalina AI, Pelletier RI, Rhodes LB. Method and apparatus of converting heat to useful energy. US 5953918; 1999.
[22] Mlcak H, Mirolli M, Hjartarson H, Ralph M. Notes form the north: a report on the debut year of the 2 MW Kalina cycle geothermal power plant in Husavik, Iceland; 2002.
[23] Nasruddin, Usvika R, Rifaldi M, Noor A. Energy and exergy analysis of kalina cycle system (KCS) 34 with mass fraction ammonia-water mixture variation. J Mech Sci Technol 2009;23:1871–6.
[24] Arslan O. Power generation from medium temperature geothermal resources: ANN-based optimization of Kalina cycle system-34. Energy 2011;36:2528–34.
[25] Lengert J. Method and device for carrying out a thermodynamic cyclic process. US patent 2007/0022753; 2007.
[26] Mergner H, Weimer T. Performance of ammonia-water based cycles for power generation from low enthalpy heat sources. Energy 2015;88:93–100.
[27] Ibrahim MB, Kovach RM. A Kalina cycle application for power generation. Energy 1993;18:961–9.
[28] Nguyen TV, Knudsen T, Larsen U, Haglind F. Thermodynamic evaluation of the Kalina split-cycle concepts for waste heat recovery applications. Energy 2014;71:277–88.
[29] He J, Liu C, Xu X, Li Y, Wu S, Xu J. Performance research on modified KCS (Kalina cycle system) 11 without throttle valve. Energy 2014;64:389–97.
[30] Hua J, Chen Y, Wu J, Zhi Z, Dong C. Waste heat supply-side power regulation with variable concentration for turbine in Kalina cycle. Appl Therm Eng 2015;91:583–90.
[31] Mlcak HA, Mirolli MD. System and methods for increasing the efficiency of a Kalina cycle. US patent 8744636; 2014.
[32] Walraven D, Laenen B, D'haeseleer W. Minimizing the levelized cost of electricity production from low-temperature geothermal heat sources with ORCs: water or air cooled? Appl Energy 2015;142:144–53.
[33] Collings P, Yu Z, Wang E. A dynamic organic Rankine cycle using a zeotropic mixture as the working fluid with composition tuning to match changing ambient conditions. Appl Energy 2016;171:581–91.
[34] Sun J, Li W. Operation optimization of an organic rankine cycle (ORC) heat recovery power plant. Appl Therm Eng 2011;31:2032–41.
[35] Chan KT, Yu FW. Applying condensing-temperature control in air-cooled reciprocating water chillers for energy efficiency. Appl Energy 2002;72:565–81.
[36] Pierobon L, Nguyen TV, Mazzucco A, Larsen U, Haglind F. Part-load performance of a wet indirectly-fired gas turbine integrated with an organic Rankine cycle turbogenerator. Energies 2014;7(12):8294–316.
[37] Lemmon EW, Huber ML, McLinden MO. NIST standard reference database 23: reference fluid thermodynamic and transport properties-REFPROP, version 9.1. Gaithersburg: National Institute of Standards and Technology; 2013. Standard Reference Data Program.
[38] Barkaoui AE, Boldyryev S, Duic N, Krajacic G, Guzovic Z. Appropriate integration of geothermal energy sources by Pinch approach: case study of Croatia. Appl Energy 2016. http://dx.doi.org/10.1016/j.apenergy.2016.04.112.
[39] Walas SM. Phase equilibria in chemical engineering. Boston: Butterworth Publishers; 1984.
[40] TuTiempo.net. Global climate data; 2015. <http://en.tutiempo.net/climate/2015.html>.